Jammer-Nulling Transmit-Adaptive Radar Against Knowledge-Based Jammers in Electronic Warfare

Q. JEANETTE O. TAN, (Member, IEEE), AND RIC A. ROMERO, (Senior Member, IEEE)
Naval Postgraduate School, Monterey, CA 93943, USA

Corresponding author: Q. Jeanette O. Tan (q.jeanette.o.tan@gmail.com)

ABSTRACT The authors present transmit-adaptive jammer nulling waveforms in cognitive radar (CRr) for aircraft response recognition as a form of electronic support in the electronic warfare domain. New forms of knowledge-based noise jammers that function as a form of electronic attack to matched illumination waveforms are also introduced. These knowledge-based noise jamming techniques capitalize on prior knowledge of the target's frequency response to obscure the true target response echo. The results from simulation show that real-time adaptive waveforms suppress the effects of electronic attack noise jammers and the newly introduced knowledge-based noise jammers. High bandwidth radar cross section (RCS) responses via electromagnetic (EM) simulations of true-to-physical-size aircraft are used for simulations to produce CRr classification performance against a comprehensive list of noise jammers.

INDEX TERMS Cognitive radar, electronic warfare, electronic support, electronic protection, electronic attack, waveform design, matched waveform, eigenwaveform, mutual information, target recognition, aircraft target.

I. INTRODUCTION

Electronic warfare (EW) involves the use of electromagnetic (EM) spectrum or directed energy to control EM spectrum for the purpose of deceiving an adversary or to protect friendly systems against similar actions. The use of experience acquired through interactions with the environment in a cognitive radar (CRr) framework to maintain stable and reliable operation mirrors the cyclic process of EW and the interactions between its subdivisions: electronic attack (EA), electronic protection (EP) and electronic support (ES). EA involves the use of EM energy (this includes radar jamming), directed energy, or anti-radiation weapons to disrupt one's ability to utilize the EM spectrum effectively. EP protects equipment, capabilities and personnel against friendly or enemy use of the EM spectrum that degrades one's system capability. ES comprises of tasks that intercept, detect, identify and localize sources of intentional or unintentional radiated EM energy for the purpose of maintaining spectrum situational awareness. Hence, ES provides information required for subsequent EA and EP planning [1]–[4].

Cognitive radar is a closed-loop knowledge-aided dynamic radar architecture designed to mimic biological cognitive properties. It has been proposed in [5] as a technological

solution for performance optimization in resource-constrained and spectrally dense environments [6], [7]. The CRr distinguishes itself from a traditional receiver-adaptive radar in that CRr adaptively modifies its transmit waveform in response to current and previous measurements from its adaptive receiver via feedback regarding the electromagnetic (EM) environment [8]. Consequently, transmit waveform design based on knowledge gained through CRr interactions with the environment including EA jammers and friendly interferences is crucial to combat EA and potentially improve performance while utilizing available resources efficiently.

The application of CRr for target system identification using adaptive waveforms was first investigated in [9]. This CRr platform utilizes energy-constrained matched illumination [10], [11] waveforms that maximize signal-to-noise ratio (SNR) and mutual information (MI) metrics for a known target in additive white Gaussian noise (AWGN). The design of signals for clutter rejection was considered in [12], [13] and signal design for Gaussian point target in Gaussian clutter was presented in [14]. The method in [13] was applied to target recognition in [15], [16]. In addition, optimal waveforms using SNR or MI-based metrics matched to deterministic or stochastic extended targets in signal-dependent interference and/or AWGN were addressed in [17]–[19]. In [20], [21] high-fidelity target model signatures were used

to demonstrate the performance of adaptive waveforms in CRr for angle discrimination and target class recognition given aspect angle deviation.

ES tasks such as target detection, target signature identification as well as target search and track using CRr architecture were presented in [9], [22]–[26]. If we were to apply target aircraft response recognition using adaptive waveforms in CRr as an ES measure in EW, it is imperative to consider the various types of EA noise jammers as significant sources of interference such that transmit-adaptive waveforms are designed to suppress/mitigate the effects of jammer interference. In our preliminary work [27], [28] we introduced jammer nulling transmit-adaptive waveforms that function as a countermeasure against narrowband, frequency sweep and base noise jammers. In this paper, we significantly expand our design to several transmit-adaptive jammer nulling waveforms in a CRr framework for aircraft radar cross section (RCS) response recognition against a substantial list of EA noise jammers.

Also, works in [9], [18], [29] considered arbitrarily generated targets which have very few frequency resonances and as such do not represent practical wideband targets. It is imperative that the next major advance in this new "CRr meets EW" topic to consider true-to-size targets whose physical extents are significant. Our EW interest is on aircraft targets but unfortunately, RCS field measurements on fighter jets and practical-sized UAVs may not be publicly available or may not come in the frequency or even bandwidth of interest. Therefore, we address this need by generating RCS responses of such targets by EM simulations at X-band with 1 GHz bandwidth using aircraft Computer-Aided Design (CAD) models. The EM field responses from these electronically large targets dictated the use of powerful computing workstations due to the immensely lengthy CAD simulations for various aspect angles but our efforts are rewarded in the "CRr meets EW" scenarios to be presented later.

It is not possible to address all types of EA noise jammers used in disrupting the EM spectra (used by various aircraft radars due to obvious proprietary reasons) but we will address several fundamental noise jammer types in this work. Therefore, another significant contribution in this paper is the inclusion of several jammer nulling transmit-adaptive waveforms that serve as a countermeasure against the EA noise jammers intended to disrupt the CRr platform's ability to correctly identify the target aircraft. In this work, we consider a comprehensive list of static, frequency-varying and/or time-varying noise jammers which include: narrowband jammer (NBJ), double-lobe NBJ, comb jammer (CMJ), frequency sweep jammer (SWJ), frequency agile jammer (FQJ), pulsed jammer (PJ) and the base jammer (BJ). The suppression or exploitation of a cadre of noise jammer spectral distributions with the use of jammer-nulling transmit-adaptive waveforms is certainly a substantial contribution in this new twist of EW application to CRr classification problems. As mentioned, this "CRr-based EP versus EA" and the adaptive transmit-waveform techniques presented

in this work are a significant advance from the traditional receiver-centric jammer mitigation techniques such as outlined in [30].

Aside from traditional EA noise jammers, we also introduce a new form of knowledge-based (KB) jammer design that capitalizes on prior knowledge of the target's frequency response. The KB noise jamming technique designed via the use of EM-simulated target responses described in this paper is a recent development (as far as we can ascertain from a thorough search of the open literature). This KB jammer is a form of multi-lobe narrowband jammer that focuses its jamming power in one or few dominant bands where the target resonances reside. The novel idea is to have the KB jammer function as an EA against the SNR and MI-based matched illumination waveforms (which have attracted substantial interest in recent years). As will be shown later, the KB jammers are very effective in obscuring the convolution of the transmit waveform and target response echo. Several KB jammer schemes can be designed as desired and/or specified. Here we introduce two: KB narrowband noise jammer (KB-NBJ) and a target-matched KB narrowband noise jammer (MKB-NBJ).

The contributions of this paper are included (but not limited to):

- introduction of transmit-adaptive jammer nulling waveforms that suppress the effects of a comprehensive list of EW noise jammers;
- CRr classification performance curves for the above waveforms are reported via extensive Monte Carlo simulations;
- the utilization of EM-simulated target responses of true-to-physical size aircraft from high fidelity CAD models for EW application;
- the introduction of a novel KB jammer noise techniques which act as EA counter measure to matched illumination;
- and the eventual use of CRr as EP against the EA KB jammers.

This paper is organized as follows. Section II describes the signal model for the "CRr meets EW" application, introduces the new knowledge-based jammer design, and reviews the CRr platform against the jammer scenario. Section III presents the jammer nulling transmit-adaptive waveform design and corresponding jammer-uncompensated transmit-adaptive waveform design based on signal-to-interference-plus-noise ratio (SINR) and MI metrics. Section IV summarizes the closed-loop radar for aircraft RCS response recognition against noise jammer interference. Section V presents the probability-weighted waveform update Bayesian methodologies and presents the SINR and MI-based matched waveforms corresponding to each type of noise jammer. Section VI describes the generation of high-fidelity practical aircraft target set and their respective EM-simulated RCS responses. Section VII summarizes the noise jammers in our work. Section VIII examines the false detections rates in the presence of KB jammer interference. The target aircraft
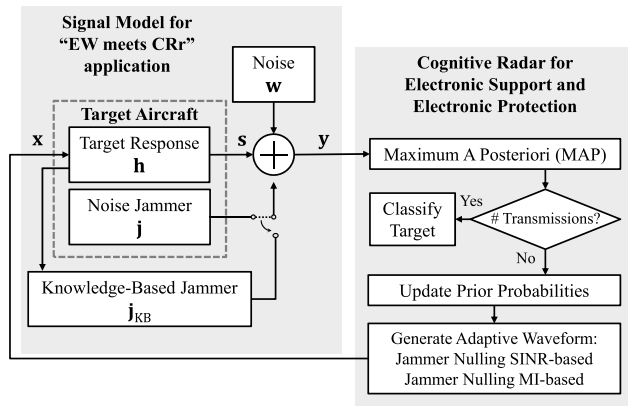
FIGURE 1. Block diagram of signal model and cognitive radar platform for target recognition using jammer nulling adaptive matched waveform design.

classification results for jammer nulling and jammer-uncompensated adaptive waveforms of various noise jammers are presented and discussed in Section IX. Lastly, Section X summarizes and concludes this paper.

II. EW MEETS CRR AND THE INTRODUCTION OF NOVEL KNOWLEDGE-BASED JAMMERS

A complex-valued baseband signal block diagram illustrating the new "EW meets CRr, with ES and EP functionalities" is shown in Figure 1. Following the convention in signal processing, continuous-time passband signals are downconverted to baseband and sampling time is normalized. Let $x[n]$ or $\mathbf{x}$ be a finite-energy complex-valued transmit waveform vector of length L with discrete Fourier transform (DFT) $X[f]$ or $\mathbf{x}(f)$ where $f = 0, 1/L, 2/L, \ldots, 1 - 1/L$. Let $\mathbf{h}$ represent a deterministic extended target with discrete Fourier transform $\mathbf{h}(f)$ which can be estimated through an initial transmission of a wideband waveform or with coarse direction finding (DF). The uncertainty arising from target response estimation can be addressed by introducing modifications to the transmit-adaptive waveform methods as presented in our previous work [21]. Let $\mathbf{w}$ be the complex-valued noise from the receiver hardware with PSD $\mathbf{p}_{nn}(f)$. Let $\mathbf{j}$ represent noise jammer interference with power spectral density (PSD) $\mathbf{p}_{jj}(f)$. The jammer may be physically located on the aircraft or at a distance from the aircraft such as a ground jammer where the signal model also applies. In Figure 1, we consider two cases: (a) the jammer transmitter is positioned on the true target hypothesis in an aircraft response recognition problem, or (b) the jammer transmitter is mounted on another aircraft or separately (e.g. ground jammer). In the first case, the target emits jammer noise directed at the CRr platform as shown in Figure 2a. The received signal plus noise jammer interference and AWGN vector is $\mathbf{y} = \mathbf{s} + \mathbf{j} + \mathbf{w}$ where the received target echo $\mathbf{s}$ is the convolution of the transmit waveform and target response ($\mathbf{s} = \mathbf{x} * \mathbf{h}$). For the second case, shown in Figure 2b, we consider a new KB noise jammer $\mathbf{j}_{KB}$ positioned on another aircraft (or ground jammer) at a distance from the target aircraft. Likewise, the received
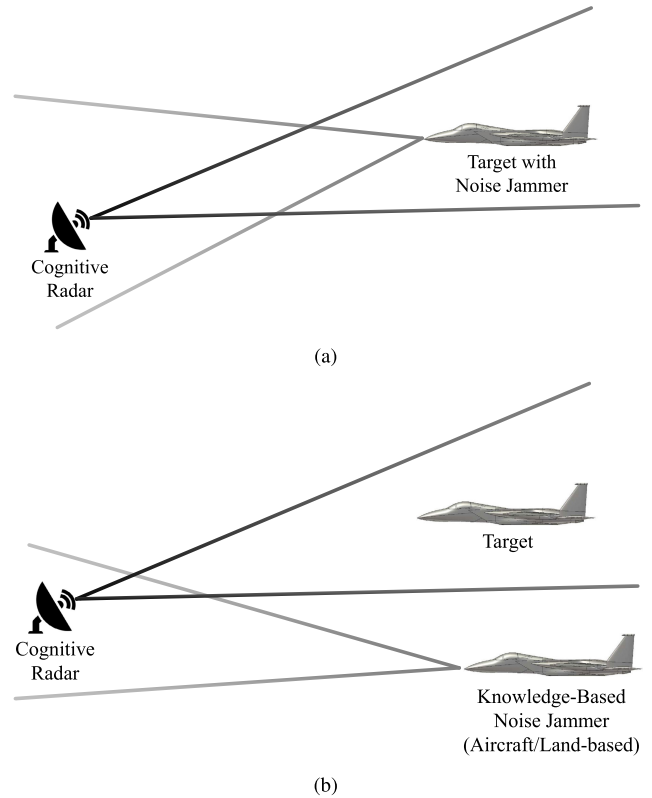
FIGURE 2. Cognitive radar with ES and EP functionalities against. (a) target with EA noise jammer, or (b) target and knowledge-based EA noise jammer set-up for aircraft response recognition.

signal plus noise jammer interference and AWGN is $\mathbf{y} = \mathbf{s} + \mathbf{j}_{KB} + \mathbf{w}$.

A. TRADITIONALLY SHAPED KNOWLEDGE-BASED NARROWBAND JAMMER

Now, we formulate the general guideline on how to form a target-directed narrowband knowledge-based jammer. Recall that a target's wideband response is given by $\mathbf{h}(f)$. The general idea is to place the noise energy at the largest resonant (i.e. the dominant) band of the target in order to obfuscate the target in a very effective way. This action is effectively an EA on a radar employing the SNR-based waveform (i.e. eigenwaveform). For the traditionally shaped KB jammer, the procedure to form a noise jammer PSD is given by the following algorithmic steps or procedure:

1) Determine the narrowband constraint B_c of the EA noise generator hardware and compare to the target's bandwidth being considered by the radar (to be jammed). For example, as a practical constraint on lower cost jammer, B_c may be a fifth (or less) of the target's frequency response.

2) Using the bandwidth constraint, find the specific band $f_1 < f \leq f_2$ that contains the target's largest energy. This can be easily accomplished by various algorithms; the simplest is producing running energy totals by moving the constrained band in the entire target's bandwidth. For example, a running average approach should

easily find the largest energy total corresponding to the bandwidth constraint.

3) Once the band $B_c = f_2 - f_1$ is found, use a traditional spectral shape to form the noise jammer PSD. For example, one can use Hamming, Blackman, etc. Let the target-directed PSD be $p_{\mathrm{KB}}(f)$.

4) Use the spectral shape on the noise generator either digitally (FPGA FIR filter) or RF-wise (with IF filter).

In other words, the KB-NBJ for the ith target is defined in the bandwidth, $f_{1,i} < f \leq f_{2,i}$, corresponding to the ith target's frequency response band containing the highest target response energy. In the results section of this work, the KB-NBJ PSD in the frequency band of $f_{1,i} < f \leq f_{2,i}$ is assumed to be a Hamming function.

For a radar performing target recognition given M possible targets, a more advanced EA jammer can form an aggregate target-directed narrowband noise jamming signal by linearly combining all the individual KB PSDs given by

$$\mathbf{p}_{jj,\mathrm{KB}}(f) = w_i \sum_{i=1}^{M} \mathbf{p}_{\mathrm{KB},i}(f), \qquad (1)$$

where $\mathbf{p}_{\mathrm{KB},i}(f)$ is the KB-NBJ PSD of the ith target and w_i is the weight assigned to that target by the EA jammers.

B. TARGET-MATCHED KNOWLEDGE-BASED NARROWBAND JAMMER

Another technique we propose is a target-matched KB narrowband noise jammer (MKB-NBJ), where the PSD of the narrowband jammer is given by

$$\mathbf{p}_{\mathrm{MKB}}(f) = \begin{cases} |\mathbf{h}(f)|, & f_1 < f \leq f_2 \\ 0, & \text{otherwise} \end{cases} \qquad (2)$$

In other words, step 3 in the traditionally-shaped KB narrowband jammer procedure is replaced by the actual shape (magnitude) of the target's frequency response in the band ($f_1 < f \leq f_2$) containing the target's largest energy. Recall that the frequency band constraint is given B_c.

For an aggregate EA noise jammer representing various targets, the KB jammer is given by

$$\mathbf{p}_{jj,\mathrm{MKB}}(f) = w_i \sum_{i=1}^{M} \mathbf{p}_{\mathrm{MKB},i}(f), \qquad (3)$$

where $\mathbf{p}_{\mathrm{MKB},i}(f)$ is the MKB-NBJ PSD of the ith target and w_i is the weight assigned by the EA noise jammer. Recall the MKB-NBJ for the ith target is defined in the bandwidth, $f_{1,i} < f \leq f_{2,i}$, corresponding to the ith target's frequency response band containing the highest target response energy.

III. JAMMER NULLING AND JAMMER-UNCOMPENSATED WAVEFORM DESIGN

We now present the fully-vectorized jammer nulling transmit-adaptive waveform design approaches that maximize SINR and MI metrics for an extended target in jammer interference and AWGN. In addition, their corresponding SNR and MI-based jammer-uncompensated transmit-adaptive waveforms are summarized. The continuous jammer-nulling and jammer-uncompensated waveform design methodology were presented in our previous works [27], [28].

A. JAMMER NULLING SINR-BASED WAVEFORM DESIGN

The SINR spectral density for a known extended target in jammer noise interference and AWGN is given by

$$\mathbf{v}_{\mathrm{SINR}}(f) = \left(|\mathbf{h}(f)|^{\circ 2} \circ |\mathbf{x}_j(f)|^{\circ 2} \right) \oslash \left(\mathbf{p}_{jj}(f) + \mathbf{p}_{nn}(f) \right), \quad (4)$$

where jammer PSD $\mathbf{p}_{jj}(f)$ is incorporated in the SINR spectrum expression. Here, the $\circ$ operator denotes Hadamard product or entry-wise multiplication where for two matrices $\mathbf{A}$ and $\mathbf{B}$ of the same dimension, the Hadamard product is defined as $(\mathbf{A} \circ \mathbf{B})_{lm} = \mathbf{A}_{lm}\mathbf{B}_{lm}$. The subscripts l and m represent the row and column index. Likewise, the $\oslash$ operator denotes Hadamard division or entry-wise division where for three matrices $\mathbf{A}$, $\mathbf{B}$ and $\mathbf{C}$ of the same dimension, the Hadamard division is defined as $\mathbf{C}_{lm} = \mathbf{A}_{lm}/\mathbf{B}_{lm}$ for $\mathbf{C} = \mathbf{A}\oslash\mathbf{B}$. Similarly, $\mathbf{A}^{\circ 2}$ denotes the Hadamard power or entry-wise exponential such that $\mathbf{B}_{lm} = \mathbf{A}_{lm}^2$ for $\mathbf{B} = \mathbf{A}^{\circ 2}$. The resulting SINR is derived from the SINR spectrum as

$$\mathrm{SINR} = \left[\mathbf{v}_{\mathrm{SINR}}^T(f)\mathbf{v}_{\mathrm{SINR}}(f) \right]^{1/2} \Delta f, \qquad (5)$$

where $\Delta f = 1/L$.

For a complete vector formulation, let $\mathbf{h} = \sqrt{E_h}\bar{\mathbf{h}}$ such that E_h is the target response energy and $\bar{\mathbf{h}}$ is the corresponding unit energy vector. Likewise, let $\mathbf{x}_j = \sqrt{E_x}\bar{\mathbf{x}}_j$ where E_x is the transmit waveform energy and $\bar{\mathbf{x}}_j$ is the unit energy vector. It follows that the received signal plus interference and noise vector can be expressed as $\mathbf{y} = \sqrt{E_h}\bar{\mathbf{h}} * \sqrt{E_x}\bar{\mathbf{x}}_j + \mathbf{j} + \mathbf{w}$. It can be shown (with some effort) that for an arbitrary transmit waveform $\mathbf{x}$, the received energy due to the target return $\mathbf{s}$ using the whitened matched filter theory is given by

$$E_r = E_x E_h \bar{\mathbf{x}}_j^\dagger \bar{\mathbf{H}}^\dagger \mathbf{R}_{jn}^{-1} \bar{\mathbf{H}} \bar{\mathbf{x}}_j = E_x E_h \bar{\mathbf{x}}_j^\dagger \bar{\mathbf{R}}_T \bar{\mathbf{x}}_j, \qquad (6)$$

where the total autocorrelation $\bar{\mathbf{R}}_T$ is a function of target convolution matrix $\bar{\mathbf{H}}$ and jammer interference-plus-noise autocorrelation $\bar{\mathbf{R}}_{jn} = \bar{\mathbf{R}}_j + \bar{\mathbf{R}}_n$ such that $\bar{\mathbf{R}}_T = \bar{\mathbf{H}}^\dagger \mathbf{R}_{jn}^{-1}\bar{\mathbf{H}}$. Recall that $\mathbf{R}_n = \sigma^2\mathbf{I}$ and $\mathbf{R}_j$ is the covariance matrix due to any jammer with PSD $\mathbf{p}_{jj}(f)$.

Notice that various received energy values are possible in (6) depending on the arbitrary transmit waveform $\mathbf{x}$. According to [11], [17], the complex-valued, finite-duration jammer-nulling waveform $\mathbf{x}_j$ that maximizes SINR criterion in (5) within the energy constraint at the receiver matched filter output is obtained using the eigendecomposition given by

$$\lambda_{\max}\hat{\mathbf{x}}_j = \bar{\mathbf{R}}_T\hat{\mathbf{x}}_j, \qquad (7)$$

where $\hat{\mathbf{x}}_j$ is the maximum eigenvector corresponding to the maximum eigenvalue λ_{max}. The waveform energy constraint to be obeyed is given by

$$||\mathbf{x}(f)||^2 \Delta f = E_x. \qquad (8)$$

By applying (7) to (6), the maximum received energy [29] over all possible waveforms is given by

$$E_{r,\lambda_{max}} = E_x E_h \bar{\mathbf{q}}_{max}^\dagger \lambda_{max} \bar{\mathbf{q}}_{max} = E_x E_h \lambda_{max}, \qquad (9)$$

where $\bar{\mathbf{q}}_{max}$ is the normalized eigenwaveform corresponding to the eigenvalue λ_{max}. The jammer nulling matched transmit waveform that maximizes the received return energy is thus expressed as a function of the normalized eigenwaveform as $\bar{\mathbf{x}}_j = \bar{\mathbf{q}}_{max}$.

B. JAMMER-UNCOMPENSATED SNR-BASED WAVEFORM DESIGN
The uncompensated SNR-based transmit-adaptive waveform is obtained by maximizing the following SNR metric

$$\mathbf{v}_{SNR}(f) = \left(|\mathbf{h}(f)|^{\circ 2} \circ |\mathbf{x}_j(f)|^{\circ 2} \right) \oslash \mathbf{p}_{nn}(f),$$

$$SNR = \left[\mathbf{v}_{SNR}^T(f) \mathbf{v}_{SNR}(f) \right]^{1/2} \Delta f, \qquad (10)$$

where the eigenwaveform can be calculated by clearly setting $\mathbf{R}_j = 0$. The SNR metric can be derived from the SINR metric in (4) and (5) by simply setting $\mathbf{p}_{jj}(f) = 0$.

C. JAMMER NULLING MI-BASED WAVEFORM DESIGN
The MI-based waveform design is an information-theoretic approach derived in [10], [11]. The MI between a Gaussian target ensemble and the received signal in the presence of jammer interference and AWGN is

$$MI_{jn} = \left[MI_{jn}^T(f) MI_{jn}(f) \right]^{1/2} \Delta f, \qquad (11)$$

where MI(f) is the MI spectral density defined by

$$MI_{jn}(f) = \ln \left[1 + \frac{1}{L} \left(|\mathbf{x}_j(f)|^{\circ 2} \circ \sigma_H^{\circ 2}(f) \right) \right.$$
$$\left. \oslash \left(\mathbf{p}_{jj}(f) + \mathbf{p}_{nn}(f) \right) \right], \qquad (12)$$

where $|\mathbf{x}_j(f)|^{\circ 2}$ is the energy spectral density (ESD) of the jammer nulling transmit waveform $\mathbf{x}_j$ and $\sigma_H^{\circ 2}(f)$ is the energy spectral variance (ESV) of length L [11].

The jammer nulling waveform that optimizes MI in (11) with respect to $|\mathbf{x}_j(f)|^{\circ 2}$ while conforming to the energy constraint in (8) is described as a waterfilling waveform

$$|\mathbf{x}_j(f)|_l^{\circ 2} = \begin{cases} \mathbf{z}_l(f), & \mathbf{z}_l(f) > 0 \\ 0, & \text{otherwise} \end{cases} \qquad (13)$$

where

$$\mathbf{z}(f) = A - \left(L \left(\mathbf{p}_{jj}(f) + \mathbf{p}_{nn}(f) \right) \oslash \sigma_H^{\circ 2}(f) \right), \qquad (14)$$

and subscript l is the index or element of any column vector.

The water-level A is determined by obeying the energy constraint

$$E_x - \frac{\delta}{2} \leq ||\mathbf{x}_j(f)||^2 \Delta f \leq E_x + \frac{\delta}{2}, \qquad (15)$$

where A can be found by simple methods such as the bisection algorithm given an error tolerance δ.

D. JAMMER-UNCOMPENSATED MI-BASED WAVEFORM DESIGN
Likewise, the uncompensated MI-based transmit-adaptive waveform is obtained by maximizing the MI metric in (11) with $\mathbf{p}_{jj}(f) = 0$ such that MI and MI spectral density for a target in noise is given by [10], [11]

$$MI_n = \left[MI_n^T(f) MI_n(f) \right]^{1/2} \Delta f,$$

$$MI_n(f) = \ln \left[1 + \frac{1}{L} \left(|\mathbf{x}_j(f)|^{\circ 2} \circ \sigma_H^{\circ 2}(f) \right) \oslash \mathbf{p}_{nn}(f) \right]. \qquad (16)$$

IV. COGNITIVE RADAR FOR AIRCRAFT RCS RESPONSE RECOGNITION
A closed-loop platform for deterministic target recognition in AWGN was proposed in [9]. Figure 1 shows the scenario where the CRr is being jammed by either a form of EA noise jammer or the newly introduced KB jammer. The CRr uses jammer-nulling adaptive waveforms as a countermeasure (for EP) and the adaptive receiver uses Bayesian learning (as a form of ES) to improve aircraft target (response) classification. The number of transmissions/iterations is fixed and maximum a posteriori (MAP) is used to determine the target decision based on the most likely hypothesis after the last waveform transmission.

Consider a target recognition problem in a multiple hypothesis testing (MHT) problem with M alternatives where the ith hypothesis is characterized by the target response $\mathbf{h}_i$ and its convolution matrix $\bar{\mathbf{H}}_i$ where $i = 1, 2, \ldots, M$. The Bayesian representation of the target hypotheses are denoted by $\mathcal{H}_1, \mathcal{H}_2, \ldots, \mathcal{H}_M$ with corresponding prior probabilities $P_1, P_2, \ldots, P_M$. The ith hypothesis is

$$\mathcal{H}_i : \mathbf{y} = \mathbf{s}_i + \mathbf{j} + \mathbf{w} = \mathbf{h}_i * \mathbf{x} + \mathbf{j} + \mathbf{w} = \sqrt{E_h} \bar{\mathbf{H}}_i \sqrt{E_x} \bar{\mathbf{x}}_i + \mathbf{j} + \mathbf{w}, \qquad (17)$$

where $\mathbf{h}_i$ is the ith target impulse response.

With jammer noise $\mathbf{j} \sim \mathcal{CN}(0, \mathbf{R}_j)$ and AWGN $\mathbf{w} \sim \mathcal{CN}(0, \sigma^2 \mathbf{I})$, the corresponding pdfs are

$$p(\mathbf{y}|\mathcal{H}_i) = \frac{1}{\pi^{L_y} \det(\mathbf{C}_{jn})} \exp \left[-(\mathbf{y} - \mathbf{s}_i)^\dagger \mathbf{C}_{jn}^{-1} (\mathbf{y} - \mathbf{s}_i) \right], \qquad (18)$$

where interference-plus-noise covariance is $\mathbf{C}_{jn} = \mathbf{R}_{jn} = \mathbf{R}_j + \sigma^2 \mathbf{I}$ and L_y is the length of received signal $\mathbf{y}$.

Speaking of the jammer plus noise correlation, a few comments have to be made depending on the scenario. For a target recognition problem, the narrowband jammer interference-plus-noise autocorrelation remains the same at every transmission due to stationary jammer frequency placement [27].

This applies to the case where a double-lobe narrowband jammer or a comb jammer is present. In contrast, a) the sweep jammer interference-plus-noise autocorrelation is determined from the jammer noise spectrum at the current transmission; b) the frequency agile jammer interference-plus-noise auto-correlation is described by the jammer noise PSD corresponding to the jammer's frequency sequence; c) the pulsed jammer interference-plus-noise autocorrelation is obtained from the jammer noise distribution for affected/jammed transmissions; and d) the base jammer interference-plus-noise autocorrelation is derived from the jammer noise distribution corresponding to each target alternative.

V. PROBABILITY-WEIGHTED UPDATE METHODS

Recall that the jammer nulling matched waveform for each target hypothesis is derived by optimizing SINR or MI-based metric. The transmit waveform is then obtained by scaling each target's optimum waveform with its corresponding hypothesis probability from (18) using the probability-weighted energy (PWE) or probability-weighted spectral density (PWSD) method.

For the PWE method, each matched waveform corresponding to a target hypothesis is scaled by its updated probability as given by

$$\mathbf{x}_{\mathrm{pwe}} = \sum_{i=1}^{M} \sqrt{P_i} \bar{\mathbf{q}}_{i,\max}, \tag{19}$$

and transmit energy constraint is accommodated by

$$\mathbf{x} = \sqrt{E_x} \frac{\mathbf{x}_{\mathrm{pwe}}}{\sqrt{E_{x_{\mathrm{pwe}}}}}. \tag{20}$$

For deterministic targets, the PWSD for all hypotheses is

$$|\mathbf{h}(f)|^2 = \sum_{i=1}^{M} Pr(\mathcal{H}_i)|\mathbf{h}_i(f)|^2 - \left| \sum_{i=1}^{M} Pr(\mathcal{H}_i)\sqrt{|\mathbf{h}_i(f)|^2} \right|^2. \tag{21}$$

where $Pr(\mathcal{H}_i)$ is the probability that the ith hypothesis is true and $|\mathbf{h}_i(f)|^2$ is the ith target ESD.

The PWSD function in (21) is used in place of target ESV in (12) to derive the matched jammer nulling waveforms based on MI criterion.

The CRr dynamically learns through previous target echoes, received jamming and iterations using a Bayesian probability update rule for the ith target at $(k + 1)$th iteration

$$P_{i,(k+1)} = \beta p(\mathbf{y}_{(k+1)}|\mathcal{H}_i)P_{i,(k)}, \tag{22}$$

where $p(\mathbf{y}_{(k)}|\mathcal{H}_i)$ is the measurement pdf after the kth iteration and β ensures unit total probability over the target classes at each iteration. Here, the subscript (k) or $(k + 1)$ denotes the iteration number.

Unlike a narrowband jammer, the sweep jammer and frequency agile jammer utilize a different frequency band for each transmission, thus the corresponding sweep or frequency agile jammer nulling SINR or MI-based waveform is obtained by replacing $\mathbf{p}_{jj}(f)$ in (4) or (12) with the jammer PSD at the kth transmission $\mathbf{p}_{jj,k}(f)$. Likewise for the
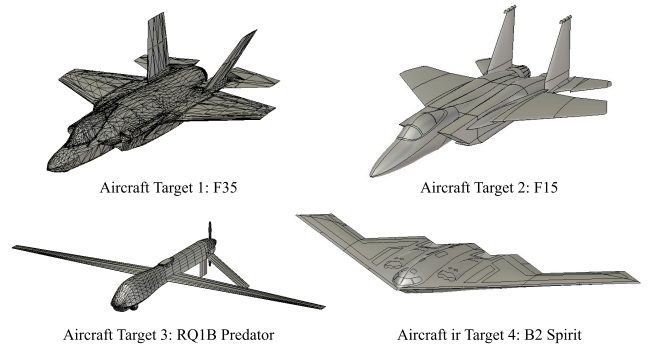
FIGURE 3. Aircraft target CAD models.

pulsed jammer nulling SINR or MI-based waveform, $\mathbf{p}_{jj}(f)$ is replaced by jammer PSD $\mathbf{p}_{jj,k}(f)$ for affected/jammed transmissions. The base jammer nulling SINR or MI-based waveform is derived by replacing $\mathbf{p}_{jj}(f)$ with the jammer PSD corresponding to the ith target alternative $\mathbf{p}_{jj,i}(f)$. For a base jammer which is only mounted on target alternative 1, $\mathbf{p}_{jj,1}(f)$ denotes the barrage jammer PSD while $\mathbf{p}_{jj,i\neq1}(f) = \mathbf{0}$. The SINR or MI-based jammer nulling waveforms utilized in the presence of KB-NBJ are obtained by replacing $\mathbf{p}_{jj}(f)$ in (4) or (12) with $\mathbf{p}_{jj,\mathrm{KB}}(f)$ in (1). Likewise, the jammer nulling waveforms used in the presence of MKB-NBJ is derived by replacing $\mathbf{p}_{jj}(f)$ in (4) or (12) with $\mathbf{p}_{jj,\mathrm{MKB}}(f)$ in (3).

VI. AIRCRAFT TARGET SET

In earlier works [9], [31]–[33], arbitrarily generated target responses consisting of few frequency resonances which are mostly distinct across different targets were used. However, these frequency responses differ greatly from practical target responses. Practical target responses consist of wide frequency components due to scattering centers and physical geometry of the targets. It is therefore imperative to use realistic aircraft target RCS signatures to ensure the validity of target recognition performance results presented.

In this paper, a set of four publicly available air vehicle Computer-Aided Design (CAD) models shown in Figure 3 are modified to actual scale and size. These publicly available CAD models are either cost free or for a fee. The models are imported to Computer Simulation Technology (CST) Microwave Studio (MWS) simulation software. The asymptotic solver that utilizes the ray tracing technique is used to generate high-fidelity EM-simulated frequency responses at head-on angle of incidence, i.e. 0° in azimuth ($\theta_{az} = 0°$) and 0° degree in elevation ($\theta_{el} = 0°$). Airborne EW receivers, like the radar warning receiver (RWR) typically operate in the 0.5 to 18 GHz frequency range with airborne intercept applications operating in the X-band (8 to 12 GHz) [34]. Hence, in this paper we consider airborne target frequency responses between 9 to 10 GHz. The 9 to 10 GHz magnitude frequency responses based on RCS generated in CST are shown in Figure 4. The frequency responses contain rich frequency components, making the wideband impulse waveform a good candidate waveform for all targets. The wideband impulse waveform will thus be used as a
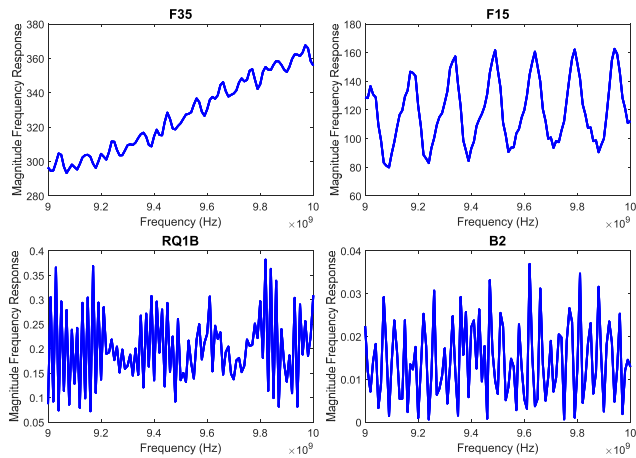
FIGURE 4. Aircraft 9-10 GHz magnitude frequency responses at $\theta_{az} = 0°$ and $\theta_{el} = 0°$.

baseline for performance comparison with adaptive waveforms presented in this paper. We note that the two fighter jets have significantly higher RCS responses than the unmanned aerial vehicle (UAV) and stealth bomber (as one may expect). The passband frequency responses are downconverted to normalized baseband impulse responses. The aircraft target impulse responses (real part) consist of delta-like functions which correspond to areas of strong returns.

VII. COMPREHENSIVE LIST OF NOISE JAMMERS

Here, we summarize the types of noise jammer interference considered. The types of noise jammers considered in this paper includes traditional [35] as well as specialized jammers specifically designed for this paper and are listed as: a) single lobe narrowband jammer, b) double-lobe narrowband jammer, c) comb jammer, d) frequency sweep jammer, e) frequency agile jammer, f) pulsed jammer, g) base jammer [36] and the newly introduced KB jammers.

A. NARROWBAND AND COMB JAMMER

Narrowband jamming (NBJ) is formed when the jammer focuses the jammer noise power in a narrow frequency band. Spot jamming is a special case of narrowband jamming where the spot noise is confined to a narrowband and concentrated at the victim system's center frequency and bandwidth. Here we consider two arbitrarily generated single lobe NBJ noise: NBJ-1 with bandwidth from 9.2-9.4 GHz and NBJ-2 with bandwidth from 9.6-9.8 GHz with jammer-to-noise ratio JNR = 20 dB and PSD $\mathbf{p}_{jj}(f)$ shown in Figure 5a and Figure 5b respectively. We also consider two other noise jammers with frequency responses that are fixed in transmission time and frequency domain: double-lobe narrowband jammer NBJ-3 and a comb jammer (CMJ) with JNR = 20 dB and PSDs are shown in Figure 5c and Figure 5d respectively.

B. FREQUENCY SWEEP AND FREQUENCY AGILE JAMMER

Frequency sweep jamming (SWJ) is a form of noise jammer where the jammer's frequency distribution is shifted
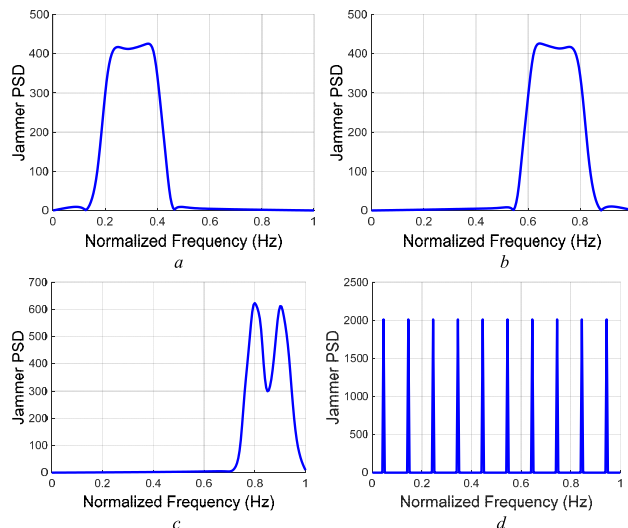

FIGURE 5. Jammer noise PSD (fixed in time) normalized in frequency corresponding to 9-10 GHz with JNR = 20 dB and AWGN set at 1W. a) Single lobe low frequency narrowband jammer NBJ-1, b) Single lobe high frequency narrowband jammer NBJ-2, c) Two lobe high frequency narrowband jammer NBJ-3, and d) comb jammer CMJ.
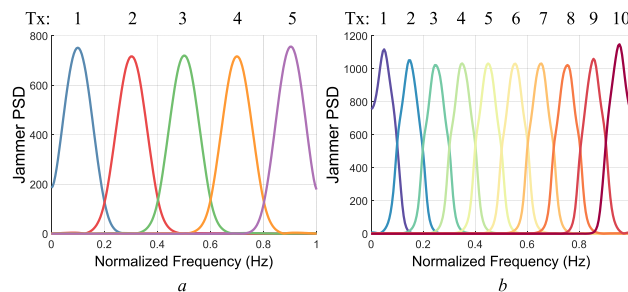

FIGURE 6. Frequency sweep jammer noise PSD normalized in frequency corresponding to 9-10 GHz with JNR = 20 dB and AWGN set at 1W. a) 5 transmissions, and b) 10 transmissions.

from one frequency to another. Here, we assume that the frequency sweep jammer noise "sweeps" through a range of frequencies while the frequency agile jammer "hops" from one frequency to another according to a pseudo-noise (PN) frequency sequence. In our work, we consider frequency sweep jammer corresponding to 5 and 10 transmissions. The frequency sweep jammer PSD with JNR = 20 dB at each transmission is shown in Figure 6. Similarly, we examine the effects of frequency agile noise jammer interference over 5 and 10 transmissions. The non-repeating frequency sequence is generated randomly over k transmissions, each with a bandwidth of $\frac{1}{k}$ Hz in normalized frequency. Figure 7 shows an example of the frequency agile jammer's frequency sequence normalized in frequency over 5 and 10 transmissions.

C. PULSE JAMMER

Pulse jammer transmits narrowband jammer noise that pulses with a period corresponding to the radar mast rotation speed or transmission cycle. Here we consider pulse jammer with a
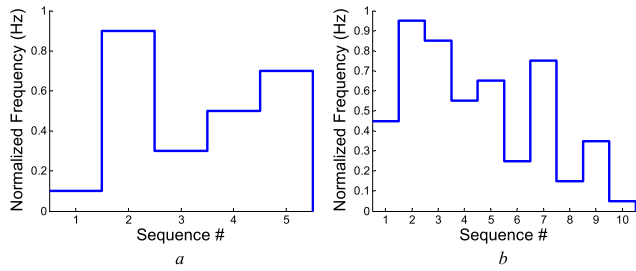
FIGURE 7. Frequency agile jammer frequency sequence normalized in frequency corresponding to 9-10 GHz. a) 5 transmissions, and b) 10 transmissions.
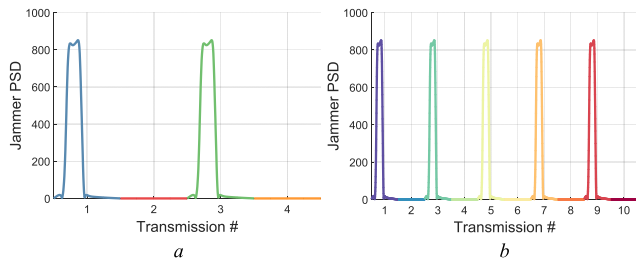
FIGURE 8. Pulse jammer PSD at each transmission. a) 4 transmissions with 0.5 duty cycle and JNR = 23 dB, and b) 10 transmissions with 0.5 duty cycle and JNR = 23 dB.

duty cycle of $\tau/\mathrm{PRI} = 0.5$ over 4 and 10 transmissions where τ denotes pulse width and PRI represents the pulse repetition interval. A lower transmit duty cycle translates to higher pulse peak power to retain the same average power. Since our duty cycle is 0.5, we let JNR = 23 dB to retain an average JNR = 20 dB. The jammer PSD at each transmission is shown in Figure 8.

D. BASE JAMMER

Base jamming is a type of barrage jamming where one radar is jammed effectively at all frequencies. In our experiments, we assume that base jammer is on the true target hypothesis in a RCS response recognition problem such that the target "present" transmits barrage jammer noise directed at the CRr platform (Figure 2).
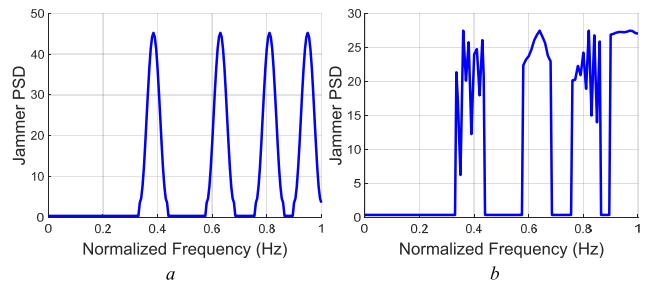
E. KNOWLEDGE-BASED JAMMERS

A traditionally shaped KB narrowband jammer is a form of narrowband jammer that utilizes knowledge regarding the possible targets a radar is searching for and their respective target frequency responses. The KB jammer focuses the jammer noise power in a narrow frequency band corresponding to the target's frequency band, B_c, containing the greatest target response energy. The B_c corresponding to each aircraft target in Figure 3 is shown in Figure 9. The KB narrowband jammer PSD for each target hypothesis is summed to derive the overall KB narrowband jammer PSD.

Here, we consider two forms of KB-NBJ. The first KB-NBJ is defined in (1), where the narrowband jammer PSD for each target is defined using the Hamming function. This KB-NBJ PSD for the four targets (Figure 3)
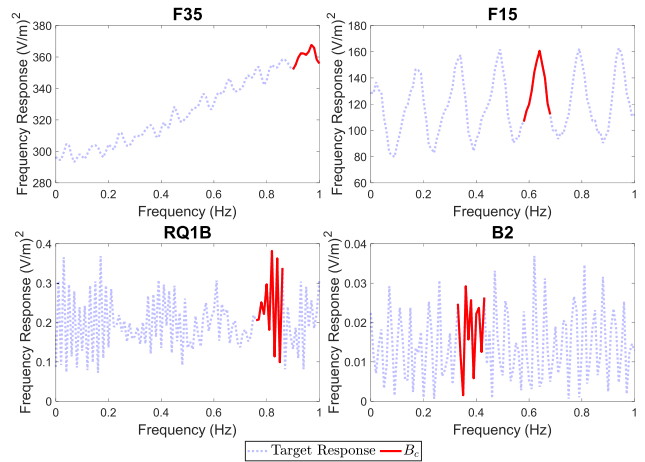
FIGURE 9. Narrowband bandwidth B_c containing the largest target response energy.

FIGURE 10. Knowledge-based jammer noise PSD normalized in frequency corresponding to 9-10 GHz with JNR = 10 dB and AWGN set at 1W. a) KB-NBJ, and b) MKB-NBJ.

with JNR = 10 dB is shown in Figure 10a. In our work, we also consider another form of knowledge-based jammer, MKB-NBJ, defined in (2), where the narrowband jammer PSD for each target is "matched" to its target's frequency response in the applicable frequency band. The MKB-NBJ PSD with JNR = 10 dB is shown in Figure 10b.

F. SUMMARY OF JAMMERS AND WAVEFORM ABBREVIATIONS

Here, we summarize the jammers, jammer nulling adaptive waveforms and jammer-uncompensated adaptive waveform abbreviations utilized in this paper.

BJ   base jammer
BJN   base jammer nulling waveform
CJN   comb jammer nulling waveform
CMJ   comb jammer
FJN   frequency agile jammer nulling waveform
FQJ   frequency agile jammer
KB   knowledge-based
KBJN   knowledge-based jammer nulling waveform
KB-NBJ   knowledge-based jammer
MI   mutual information
MKBJN   target-matched knowledge-based jammer nulling waveform
MKB-NBJ   target-matched knowledge-based jammer

NBJ	narrowband jammer
NJN	narrowband jammer nulling waveform
PJ	pulsed jammer
PJN	pulsed jammer nulling waveform
PWE	probability-weighted energy
PWSD	probability-weighted spectral density
SINR	signal-to-interference-plus-noise ratio
SJN	frequency sweep jammer nulling waveform
SNR	signal-to-noise ratio
SWJ	frequency sweep jammer
WI	wideband waveform (receiver adaptive)

For example, the NJN-SINR-PWE is the narrowband jammer nulling waveform derived via the SINR metric and is updated by the PWE method at every transmission. Likewise, the SINR-PWE is the jammer-uncompensated equivalent waveform obtained via the SINR metric and is updated by the PWE method.

## VIII. FALSE DETECTION RATES DUE TO KNOWLEDGE-BASED JAMMER INTERFERENCES

To investigate the impact of the new knowledge-based jammers, we examine the false detection rates (F_d) when the received signal consist of only the knowledge-based jammer interference and AWGN. Here, we consider matched filter detectors that utilize wideband waveform (receiver adaptive) (WI), SNR and MI waveforms corresponding to each aircraft target shown in Figure 3, and detection thresholds derived from various probability of false alarm (P_{fa}). The detection threshold is given by

$$\gamma = Q^{-1}(P_{fa})\sqrt{\frac{E_h E_x |\bar{\mathbf{x}}^H \bar{\mathbf{R}}_h \bar{\mathbf{x}}|}{2}}, \quad (23)$$

where $\bar{\mathbf{R}}_h = \bar{\mathbf{H}}^\dagger \bar{\mathbf{H}}$ is the autocorrelation of the target convolution matrix $\bar{\mathbf{H}}$. The false detection curves against JNR for a transmit waveform energy $E_x = 0$ dBW/Hz are generated over 10,000 Monte Carlo simulations.

We examine the false detection rates with various waveform detectors matched to aircraft target responses at head on incidence (i.e., $\theta_{az} = 0°$ and $\theta_{el} = 0°$). The match filter is a function of the transmit waveform **x** and the target response **h**. The F_d curves for WI, SNR and MI matched filter detectors in the presence of KB-NBJ interference at various JNR are shown in Figure 11. Likewise, the F_d curves for WI, SNR and MI matched filter detectors in the presence of MKB-NBJ interference are shown in Figure 12. In both cases, the false detections increase with JNR and this observation is more pronounced for air targets 1 and 3. The detector that uses SNR-based matched filter produces the greatest F_d for targets 1 and 3 but one of the lowest F_d for targets 2 and 4. It is noted that a detector using detection threshold derived from a lower P_{fa} constraint results in lower F_d.

Target detection is an enabling ES task to ensure EM situational awareness and subsequent EA/EP planning for the purpose of maintaining spectrum dominance.
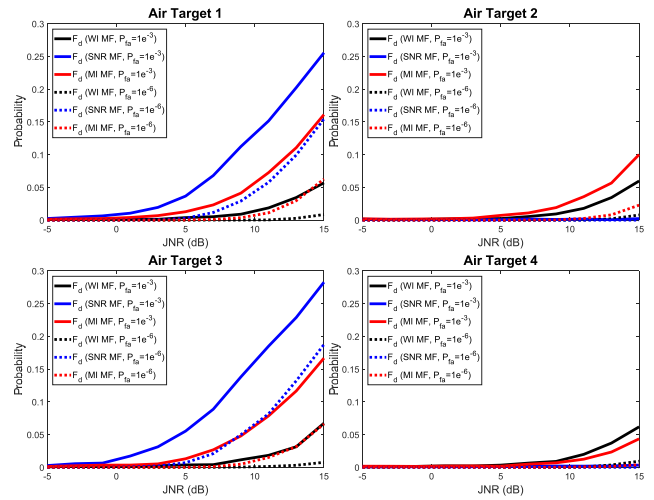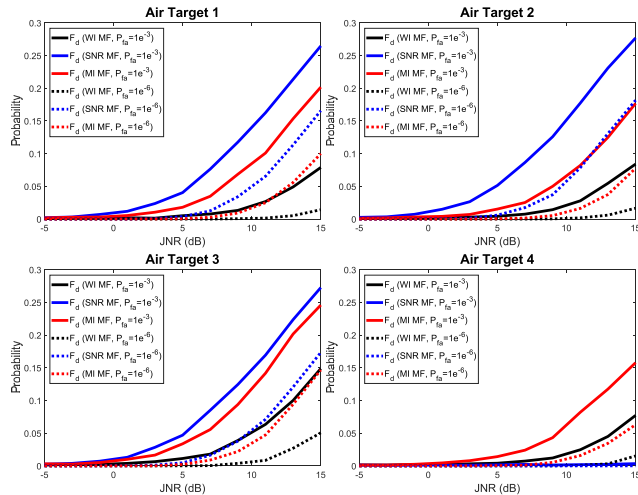

FIGURE 11. False detection rates for WI, SNR and MI waveform matched filter with P_{fa} of $1e^{-3}$ and $1e^{-6}$ when received signal comprises of KB-NBJ interference and AWGN. Aircraft target responses at $\theta_{az} = 0°$ and $\theta_{el} = 0°$ are considered.
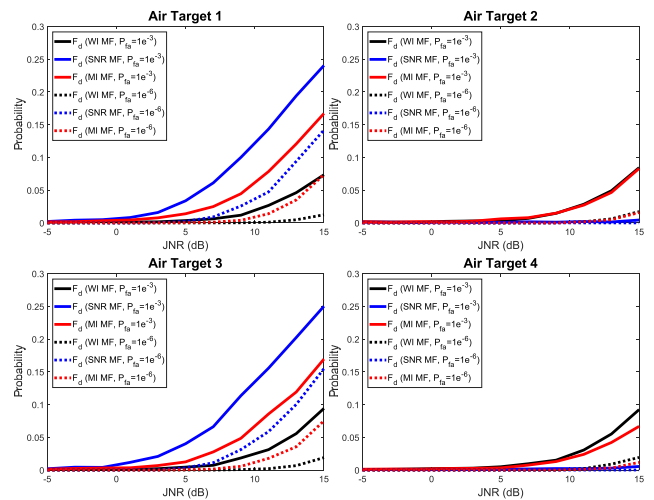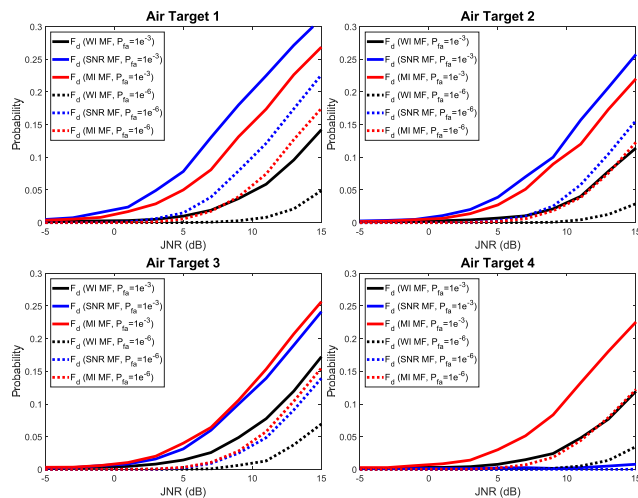

FIGURE 12. False detection rates for WI, SNR and MI waveform matched filter with P_{fa} of $1e^{-3}$ and $1e^{-6}$ when received signal comprises of MKB-NBJ interference and AWGN. Aircraft target responses at $\theta_{az} = 0°$ and $\theta_{el} = 0°$ are considered.

False detections as a result of noise jammer interference serve to undermine the interactions between the EW subdivisions resulting in erroneous reaction to the EM environment. A high F_d here suggests that the KB-NBJ and MKB-NBJ introduced in our work are effective in obscuring the true aircraft target responses if they were to be used by the adversary as EA noise jammers. In this work, we utilize the transmit-adaptive waveforms as countermeasures to these newly introduced but clearly effective jammers.

Next we present the false detection rates from utilizing waveform detectors matched to aircraft target responses at $\theta_{az} = 45°$ and $\theta_{el} = 0°$. The F_d curves for WI, SNR and MI matched filter detectors in the presence of KB-NBJ interference at various JNR are shown in Figure 13. Likewise, the F_d curves for WI, SNR and MI matched filter detec-

FIGURE 13. False detection rates for WI, SNR and MI waveform matched filter with P_{fa} of $1e^{-3}$ and $1e^{-6}$ when received signal comprises of KB-NBJ interference and AWGN. Aircraft target responses at $\theta_{az} = 45°$ and $\theta_{el} = 0°$ are considered.

FIGURE 14. False detection rates for WI, SNR and MI waveform matched filter with P_{fa} of $1e^{-3}$ and $1e^{-6}$ when received signal comprises of MKB-NBJ interference and AWGN. Aircraft target responses at $\theta_{az} = 45°$ and $\theta_{el} = 0°$ are considered.

tors in the presence of MKB-NBJ interference are shown in Figure 14. Similarly, the false detections increases with JNR. The detector that uses SNR matched filter produces the greatest F_d for air targets 1 and 2 but one of the lowest F_d for air target 4. It is observed that using target responses at $\theta_{az} = 45°$ result in higher F_d for targets 2 and 4 compared to using using target responses at $\theta_{az} = 0°$.

As seen in Figure 11 to 14, the KB jammers results in false detection rates that are at least 4 orders of magnitude worse than the specified P_{fa}, which is aggravated as JNR increases. As such, we will investigate the classification performance of jammer nulling waveforms in the presence of knowledge-based jammers and compare their performance against jammer-uncompensated waveforms.

IX. AIRCRAFT RCS RECOGNITION RESULTS

We now present the RCS response recognition performance results of CRr utilizing transmit-adaptive waveforms for aircraft response recognition in the presence of jammer interference and noise. Here, we assume that only one type of noise jammer is present with AWGN in each experiment even though it is clear that various jammers can be added simultaneously. Although such extension can be interesting, it should easily be accommodated by the signal modeling above. The number of transmissions by the closed-loop system is parameterized and MAP detection rule is used to classify the target where the target with the highest hypothesis probability is selected as the system's decision after the last transmission. Percentage of correct classification (P_{cd}) against transmit-SNR is used as a metric to quantify and compare jammer nulling adaptive waveform performance against their uncompensated counterparts and the receive-adaptive wideband pulsed waveform. We define transmit-SNR as function of transmit energy and AWGN variance such that transmit-SNR $= E_x/\sigma^2$. The four aircraft target impulse responses derived from the frequency responses in Figure 4 are used as target responses in our experiments to generate P_{cd} against transmit waveform energy E_x over 50,000 Monte Carlo simulations.
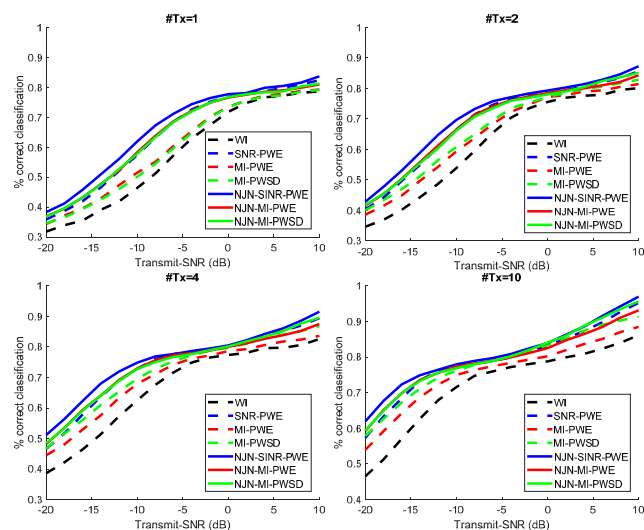
A. JAMMER NULLING ADAPTIVE WAVEFORM PERFORMANCE IN NARROWBAND JAMMER NOISE

Here we present the classification performance for narrowband jammer nulling adaptive waveforms (NJN) with CRr in the presence of narrowband jammer noise and AWGN. Three types of narrowband jammers are considered: a) single lobe low frequency narrowband jammer (NBJ-1), b) single lobe high frequency narrowband jammer (NBJ-2), and c) double-lobe narrowband jammer (NBJ-3) with PSD shown in Figure 5a-c. The target response frequencies affected by the narrowband jammers are illustrated in Figure 15 where jammer frequency distribution magnitude relative to the target response magnitude are not to scale. The jammer-to-target ratio (JTR) for each target is $JTR_{F35} = 15$ dB, $JTR_{F15} = 19$ dB, $JTR_{RQ1B} = 47$ dB and $JTR_{B2} = 58$ dB. We note that the JTR is clearly different for each target since the targets have varying effective RCS (power) as mentioned before and clearly illustrated in Figure 4. Regardless, it is clear that the effective jammer power is intended to be significantly larger than any of the target's effective RCS (power) to reflect large practical EW jammers in the field. The performance of narrowband jammer nulling adaptive waveforms: a) NJN-SINR-PWE, b) NJN-MI-PWE, c) NJN-MI-PWSD are compared against their jammer-uncompensated counterparts: a) SNR-PWE, b) MI-PWE, c) MI-PWSD and the WI waveform. Single and multiple transmissions are considered where the number of transmissions #Tx = 1, 2, 4, 10.

The classification performance of jammer nulling adaptive waveforms and jammer-uncompensated waveforms in the presence of single lobe low frequency narrowband jammer noise NBJ-1 and AWGN is shown in
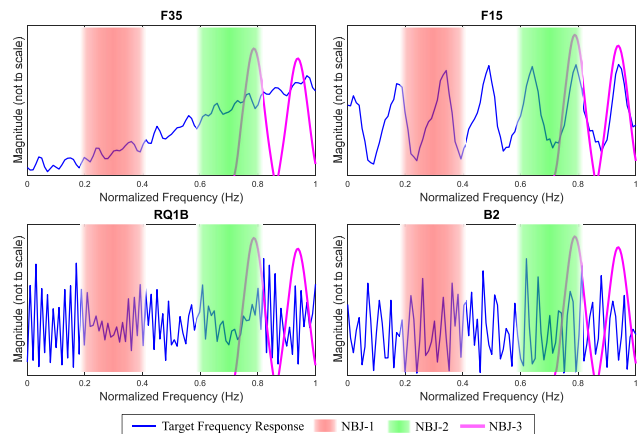
FIGURE 15. Air target frequency responses normalized in frequency corresponding to 9-10 GHz with single lobe narrowband jammer frequency distribution NBJ-1 and NBJ-2 and double-lobe narrowband jammer frequency distribution NBJ-3.

FIGURE 16. Classification performance comparison for jammer nulling adaptive waveforms (NJN-SINR-PWE, NJN-MI-PWE and NJN-MI-PWSD) with uncompensated counterparts (SNR-PWE, MI-PWE and MI-PWSD) and the wideband impulse waveform (WI) in the presence of low frequency single lobe NBJ-1 and AWGN.

Figure 16. The jammer nulling waveforms generally outperform their jammer-uncompensated counterparts at all transmit energy levels for single and multiple transmissions (e.g. NJN-SINR-PWE outperform SNR-PWE, NJN-MI-PWE outperform MI-PWE and NJN-MI-PWSD outperform MI-PWSD) with NJN-SINR-PWE achieving the best classification performance at low transmit energies. The performance gain of NJN-SINR-PWE and NJN-MI-PWSD over their jammer-uncompensated counterparts reduces at higher transmit energy levels. Note that the jammer-uncompensated SNR-PWE achieves a similar P_{cd} as the jammer nulling NJN-MI-PWE and NJN-MI-PWSD in most cases. For the jammer-uncompensated waveforms, the transmit-adaptive waveforms (SNR-PWE, MI-PWE and MI-PWSD) outperform the WI waveform in most cases.
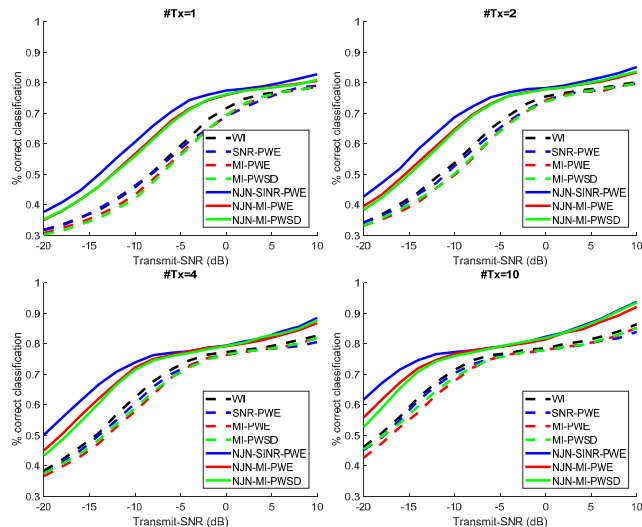
FIGURE 17. Classification performance comparison for jammer nulling adaptive waveforms (NJN-SINR-PWE, NJN-MI-PWE and NJN-MI-PWSD) with uncompensated counterparts (SNR-PWE, MI-PWE and MI-PWSD) and the wideband impulse waveform (WI) in the presence of high frequency single lobe NBJ-2 and AWGN.

Likewise, the classification performance of jammer nulling and jammer-uncompensated waveforms in the presence of single lobe high frequency narrowband jammer NBJ-2 and AWGN is shown in Figure 17. Unlike the previous case where NBJ-1 is present, all jammer nulling waveforms here outperform the jammer-uncompensated waveforms for single and multiple transmissions. The NJN-SNR-PWE waveform achieves a performance gain of 6 dB over the SNR-PWE waveform at $P_{cd} = 0.70$ in the presence of NBJ-2; and a performance gain of 2 dB at $P_{cd} = 0.70$ in the presence of NBJ-1. The improvement in classification performance of jammer nulling adaptive waveforms over their uncompensated counterparts is more pronounced in the presence of higher frequency NBJ-2 noise where significant target response frequency components are affected (see Figure 15). For this same reason, the WI waveform outperforms the jammer-uncompensated transmit-adaptive waveforms marginally in the presence of NBJ-2. Nevertheless, by incorporating SINR and MI-based jammer nulling waveforms in CRr, classification performance improves significantly with the NJN-SNR-PWE achieving the best P_{cd} at low transmit energies and all jammer nulling waveforms achieving a similar performance at higher transmit energies.

Referring to the frequency response for larger targets (F35 and F15) in Figure 16, notice that a greater amount of response energy is present at higher frequencies. Hence, we now consider a high frequency double-lobe jammer NBJ-3 where each lobe is placed such that it ''masks'' or ''jams'' the significant portions of the target frequency response of the F15. The classification performance of jammer nulling and jammer-uncompensated waveforms in the presence of high frequency double-lobe jammer NBJ-3 and AWGN is shown in Figure 18. The jammer-uncompensated
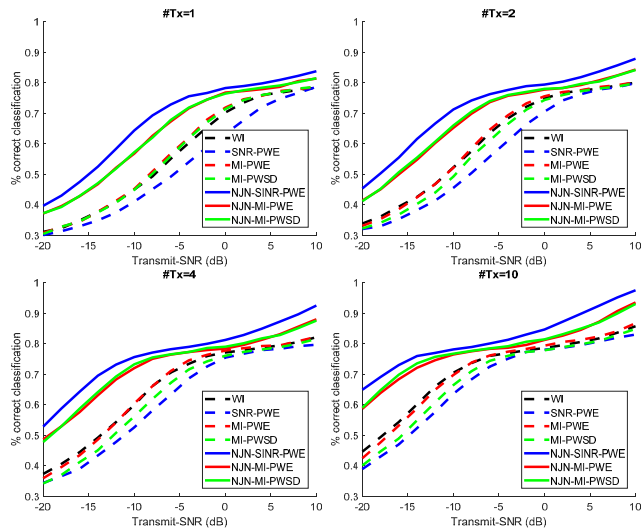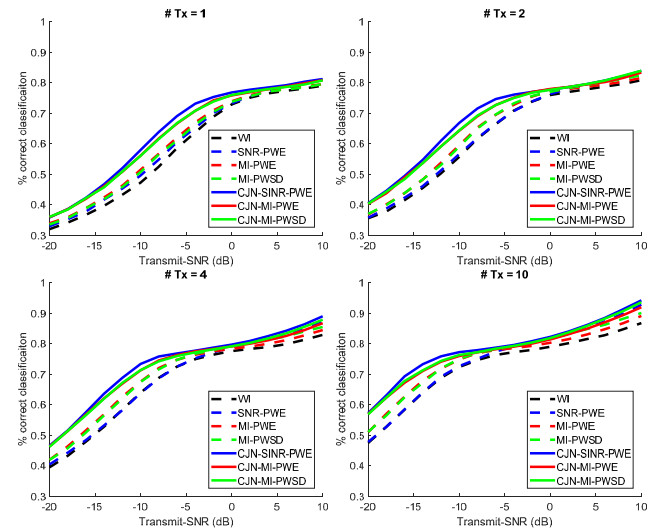
FIGURE 18. Classification performance comparison for jammer nulling adaptive waveforms (NJN-SINR-PWE, NJN-MI-PWE and NJN-MI-PWSD) with uncompensated counterparts (SNR-PWE, MI-PWE and MI-PWSD) and the wideband impulse waveform (WI) in the presence of double-lobe NBJ-3 and AWGN.

transmit adaptive waveforms' (SNR-PWE, MI-PWE and MI-PWSD) performances are greatly affected by the presence of NBJ-3. In contrast the case where NBJ-2 is present (see Figure 17), the WI achieves a greater performance gain over the jammer-uncompensated waveforms in the presence of NBJ-3. Nevertheless, classification performance improves significantly when jammer nulling waveforms are utilized with NJN-SNR-PWE achieving the best classification performance at all transmit energy levels for single and multiple transmissions. At $P_{cd} = 0.70$, the NJN-MI-PWE and NJN-MI-PWSD achieves a performance gain of $4 - 8$ dB over their jammer-uncompensated counterparts (MI-PWE and MI-PWSD) while the NJN-SNR-PWE maintains a performance gain of $\geq$ 10 dB over the SNR-PWE waveform.

B. JAMMER NULLING ADAPTIVE WAVEFORM PERFORMANCE IN COMB JAMMER NOISE

We now consider the classification performance of comb jammer nulling adaptive waveforms (CJN) with CRr in the presence of comb jammer noise as shown in Figure 5d and AWGN. The classification performance of jammer nulling adaptive waveforms: a) CJN-SINR-PWE, b) CJN -MI-PWE, c) CJN -MI-PWSD; jammer-uncompensated waveforms: a) SNR-PWE, b) MI-PWE, c) MI-PWSD and the WI waveform in the presence of comb jammer noise CMJ and AWGN is shown in Figure 19. The jammer nulling adaptive waveforms outperform jammer uncompensated waveforms, producing a greater performance gain over their uncompensated counterparts at lower transmit energy levels. The classification performance of all jammer nulling waveforms are comparable with the CJN-SINR-PWE achieving a better P_{cd} over CJN -MI-PWE and CJN -MI-PWSD at lower transmit energies.
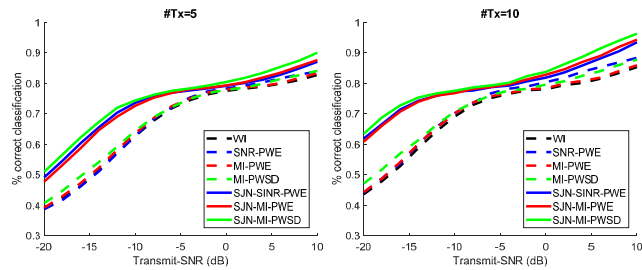

FIGURE 19. Classification performance comparison for jammer nulling adaptive waveforms (CJN-SINR-PWE, CJN-MI-PWE and CJN-MI-PWSD) with uncompensated counterparts (SNR-PWE, MI-PWE and MI-PWSD) and the wideband impulse waveform (WI) in the presence of comb jammer CMJ and AWGN.

C. JAMMER NULLING ADAPTIVE WAVEFORM PERFORMANCE IN FREQUENCY SWEEP JAMMER NOISE
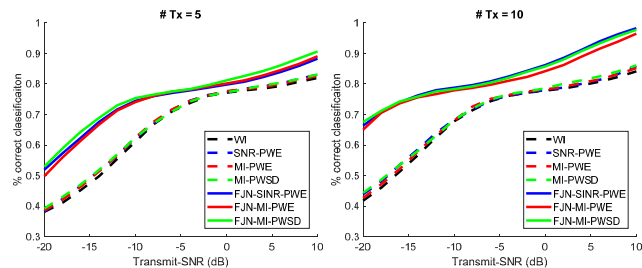
We now present the classification performance for frequency sweep jammer nulling adaptive waveforms (SJN) with CRr in the presence of frequency sweep jammer noise and AWGN. Here we consider a frequency sweep jammer which covers the entire normalized frequency band over 5 and 10 transmissions as illustrated in Figure 6. The performance of sweep jammer nulling adaptive waveforms: a) SJN-SINR-PWE, b) SJN-MI-PWE, c) SJN-MI-PWSD are compared against their jammer-uncompensated counterparts: a) SNR-PWE, b) MI-PWE, c) MI-PWSD and the WI waveform. The classification performance of jammer nulling adaptive waveforms and jammer-uncompensated waveforms in the presence of sweep jammer noise SWJ and AWGN is shown in Figure 20. The jammer nulling adaptive waveforms outperform jammer uncompensated waveforms, achieving a greater performance gain over their uncompensated counterparts at lower transmit energy levels. At $P_{cd} = 0.70$, jammer nulling waveforms produce performance gains of approximately 6 dB with 5 transmissions and 8 dB with 10 transmissions. The classification performance of all jammer nulling waveforms are similar with the SJN-MI-PWSD achieving a marginally better P_{cd} over SJN-SNR-PWE and SJN-MI-PWE. Likewise, the performance of jammer-uncompensated waveforms are comparable with the SJN-MI-PWSD and SJN-SNR-PWE outperforming the WI and SJN-MI-PWE slightly.

D. JAMMER NULLING ADAPTIVE WAVEFORM PERFORMANCE IN FREQUENCY AGILE JAMMER NOISE

Here we present the classification performance for frequency agile jammer nulling adaptive waveforms (FJN) with CRr in the presence of frequency agile jammer noise and AWGN. We consider a frequency agile jammer with
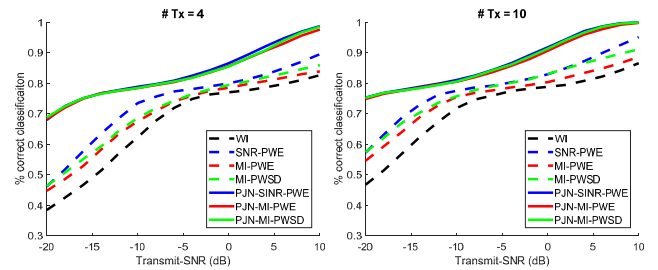
FIGURE 20. Classification performance comparison for jammer nulling adaptive waveforms (SJN-SINR-PWE, SJN-MI-PWE and SJN-MI-PWSD) with uncompensated counterparts (SNR-PWE, MI-PWE and MI-PWSD) and the wideband impulse waveform (WI) in the presence of SWJ and AWGN over 5 and 10 transmissions.

FIGURE 21. Classification performance comparison for jammer nulling adaptive waveforms (FJN-SINR-PWE, FJN-MI-PWE and FJN-MI-PWSD) with uncompensated counterparts (SNR-PWE, MI-PWE and MI-PWSD) and the wideband impulse waveform (WI) in the presence of FQJ and AWGN over 5 and 10 transmissions.

a frequency sequence that covers the entire normalized frequency band over 5 and 10 transmissions as shown in Figure 7. The performance of frequency agile jammer nulling adaptive waveforms: a) FJN-SINR-PWE, b) FJN -MI-PWE, c) FJN -MI-PWSD are compared against their jammer-uncompensated counterparts: a) SNR-PWE, b) MI-PWE, c) MI-PWSD and the WI waveform. The classification performance of the jammer nulling adaptive waveforms and jammer-uncompensated waveforms in the presence of frequency agile jammer noise FQJ and AWGN is shown in Figure 21. The jammer nulling adaptive waveforms outperform jammer uncompensated waveforms for both 5 and 10 transmissions. With 5 transmissions, the FJN-MI-PWSD outperform the FJN-SNR-PWE and FJN-MI-PWE waveforms marginally at certain transmit energy levels. The jammer nulling waveforms achieve a classification performance gain of 6 dB over the uncompensated counterparts at $P_{cd} = 0.70$. Likewise, with 10 transmissions, the FJN-MI-PWSD and FJN-SNR-PWE outperform the FJN-MI-PWE waveform slightly are higher transmit energies. In this case, the jammer nulling waveforms achieve a 8 dB performance gain over the uncompensated counterparts at $P_{cd} = 0.70$.

It is worth noting that the relative classification performance of all waveforms in the presence of frequency sweep jammer noise (Figure 20) or frequency agile jammer noise (Figure 21) are similar. In both cases, all jammer-uncompensated waveforms exhibit comparable classification performance; likewise, all jammer nulling

FIGURE 22. Classification performance comparison for jammer nulling adaptive waveforms (PJN-SINR-PWE, PJN-MI-PWE and PJN-MI-PWSD) with uncompensated counterparts (SNR-PWE, MI-PWE and MI-PWSD) and the wideband impulse waveform (WI) in the presence of PJ (JNR = 23 dB and duty cycle of 0.5) and AWGN over 4 and 10 transmissions.

waveforms achieve similar classification performance. Also in both cases, the jammer nulling waveforms outperform their jammer-uncompensated counterparts, producing significant performance gains at lower transmit energies.

E. JAMMER NULLING ADAPTIVE WAVEFORM PERFORMANCE IN PULSE JAMMER NOISE

Here, consider the classification performance for pulsed jammer nulling adaptive waveforms (PJN) with CRr in the presence of pulse jammer noise and AWGN. As illustrated in Figure 8, the pulsed jammer noise transmits with a duty cycle of 0.5, a higher jammer power (JNR = 23 dB) and has a fixed frequency distribution at every transmission. The classification performance of pulse jammer nulling adaptive waveforms: a) PJN-SINR-PWE, b) PJN -MI-PWE, c) PJN -MI-PWSD are compared against their jammer-uncompensated counterparts: a) SNR-PWE, b) MI-PWE, c) MI-PWSD and the WI waveform. The performance of jammer nulling adaptive waveforms and jammer-uncompensated waveforms in the presence of pulse jammer noise PJ and AWGN is shown in Figure 22. The jammer nulling adaptive waveforms outperform the jammer uncompensated waveforms across all transmit energies, for 4 and 10 transmissions. At 4 transmissions, the jammer nulling waveforms achieve a $8 - 10$ dB performance gain over their jammer-uncompensated counterparts at $P_{cd} = 0.80$. Likewise at 10 transmissions, the jammer nulling waveforms achieve a $7 - 10$ dB performance gain over the uncompensated counterparts at $P_{cd} = 0.80$. In both cases, the JN-MI-PWE waveform produced the highest performance gain of 10 dB over its uncompensated MI-PWE waveform. While all 3 pulse jammer nulling waveforms have comparable classification performance; the jammer-uncompensated transmit adaptive waveforms (SNR-PWE, MI-PWE, MI-PWSD) produced noticeable performance improvements over the receive-adaptive WI waveform.

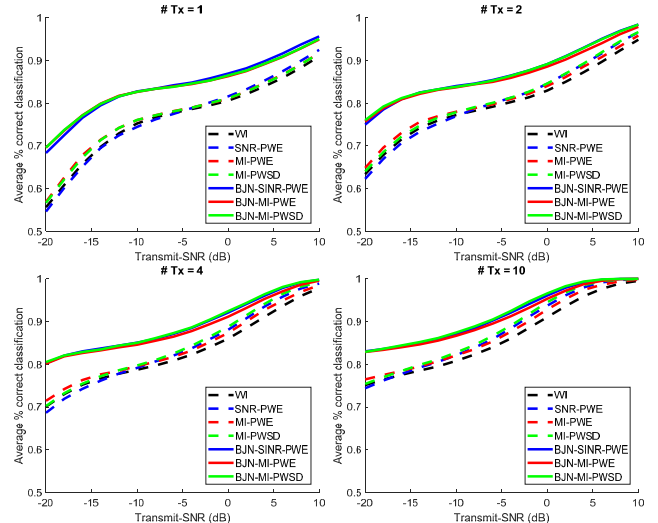### F. JAMMER NULLING ADAPTIVE WAVEFORM PERFORMANCE IN BASE JAMMER NOISE

We now consider the case where the CRr system is jammed at all frequencies by a base jammer mounted on 1 out of
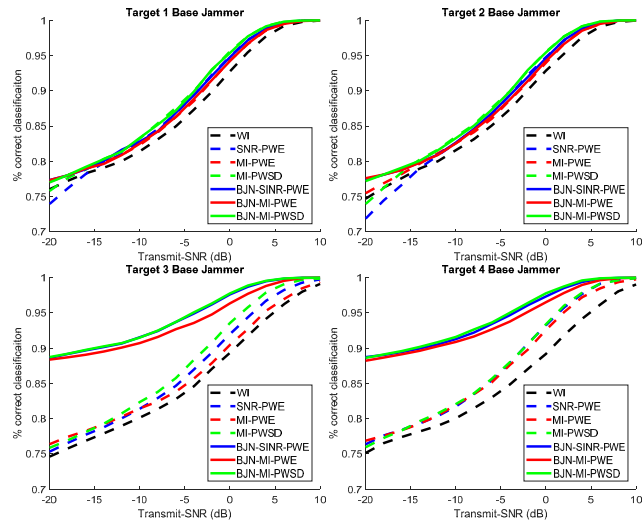
FIGURE 23. Classification performance comparison for jammer nulling adaptive waveforms (BJN-SINR-PWE, BJN-MI-PWE and BJN-MI-PWSD) with uncompensated counterparts (SNR-PWE, MI-PWE and MI-PWSD) and the wideband impulse waveform (WI) over 10 transmissions for base jammer on each target hypothesis.
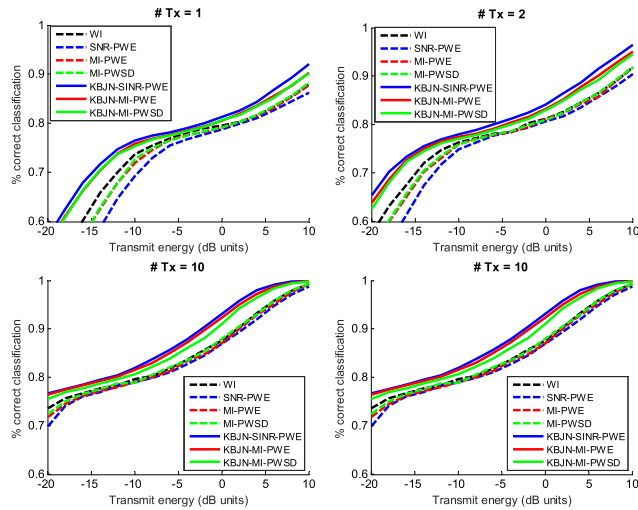

FIGURE 24. Average classification performance comparison for jammer nulling adaptive waveforms (BJN-SINR-PWE, BJN-MI-PWE and BJN-MI-PWSD) with uncompensated counterparts (SNR-PWE, MI-PWE and MI-PWSD) and the wideband impulse waveform (WI) in the presence BJ and AWGN.

the 4 possible target alternatives in Figure 3 with JNR = 20 dB. The performance of base jammer nulling adaptive waveforms (BJN): a) BJN-SINR-PWE, b) BJN -MI-PWE, c) BJN -MI-PWSD; their jammer-uncompensated counterparts: a) SNR-PWE, b) MI-PWE, c) MI-PWSD and the WI waveform in the presence of BJ noise from a fixed target over 10 transmissions is shown in Figure 23. When the base jammer noise is transmitted by targets (target 1 and target 2) with larger RCS response (see Figure 4), the jammer nulling waveforms' performance is marginally better than that of jammer-uncompensated and the WI waveform at low transmit energies but is otherwise comparable at other transmit energy levels. In contrast, for base jammer noise transmitted by targets (target 3 and target 4) with smaller RCS response (see Figure 4), the jammer nulling waveforms outperform the jammer-uncompensated and WI waveforms significantly at all transmit energies. In the case where the base jammer is mounted on target 3 or target 4, the jammer nulling waveforms achieve a performance gain of 6 dB over their jammer-uncompensated counterparts at $P_{cd} = 0.95$.

To better evaluate the overall performance of base jammer nulling adaptive waveforms over 4 target alternatives, the average percentage of correct classification is shown in Figure 24 for single and multiple transmissions #Tx = 1, 2, 4, 10. On average, the base jammer nulling waveforms outperform the jammer-uncompensated and WI waveforms with the BJN-MI-PWSD performing marginally better than the BJN-SNR-PWE and SJN-MI-PWE with greater number of transmissions. With a single transmission, all 3 jammer nulling waveforms produce comparable average classification performance. At $P_{cd} = 0.90$, the jammer nulling waveforms achieve a performance gain of approximately 4 dB over their jammer-uncompensated counterparts for single and multiple transmissions.
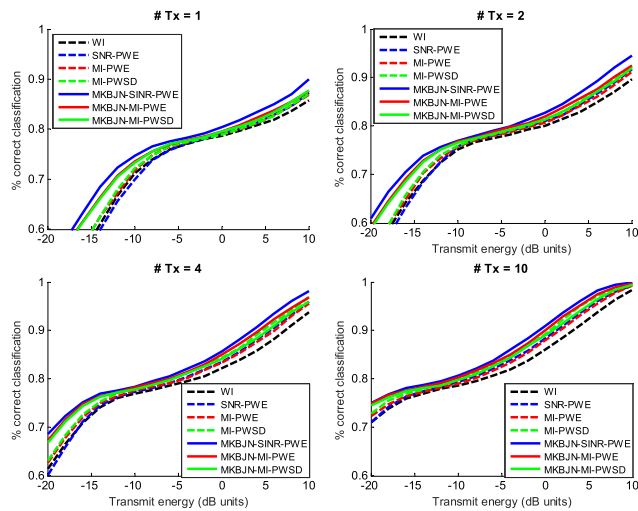
G. JAMMER NULLING ADAPTIVE WAVEFORM PERFORMANCE IN KNOWLEDGE-BASED NARROWBAND JAMMER NOISE

We now consider the classification performance of knowledge-based jammer nulling adaptive waveforms (KBJN) with CRr in the presence of KB-NBJ as shown in Figure 10a and AWGN. The classification performance of jammer nulling adaptive waveforms: a) KBJN-SINR-PWE, b) KBJN-MI-PWE, c) KBJN -MI-PWSD; jammer-uncompensated waveforms: a) SNR-PWE, b) MI-PWE, c) MI-PWSD and the WI waveform in the presence of KB-NBJ is shown in Figure 25. The jammer nulling adaptive waveforms outperform jammer uncompensated waveforms in all cases with the KBJN-SINR-PWE achieving a slightly better classification performance over other jammer nulling waveforms. At $P_{cd} = 0.80$, the KBJN-SINR-PWE achieves a performance gain of 4 dB over its jammer uncompensated counterpart with a single transmission. Likewise with multiple transmission, the KBJN-SINR-PWE achieves a performance gain of 6 dB over its jammer uncompensated counterpart at $P_{cd} = 0.80$.

Next, we consider the classification performance of target-matched knowledge-based jammer nulling adaptive waveforms (MKBJN) with CRr in the presence of MKB-NBJ as shown in Figure 10b and AWGN. The classification performance of jammer nulling adaptive waveforms: a) MKBJN-SINR-PWE, b) MKBJN -MI-PWE, c) MKBJN -MI-PWSD; jammer-uncompensated waveforms: a) SNR-PWE, b) MI-PWE, c) MI-PWSD and the WI waveform in the presence of MKB-NBJ and AWGN is shown in Figure 26. The jammer nulling adaptive waveforms outperform jammer uncompensated waveforms in all cases with the MKBJN-SINR-PWE achieving a marginally better classification performance over other jammer nulling waveforms.

FIGURE 25. Classification performance comparison for jammer nulling adaptive waveforms (KBJN-SINR-PWE, KBJN-MI-PWE and KBJN-MI-PWSD) with uncompensated counterparts (SNR-PWE, MI-PWE and MI-PWSD) and the wideband impulse waveform (WI) in the presence of KB-NBJ.

FIGURE 26. Classification performance comparison for jammer nulling adaptive waveforms (MKBJN-SINR-PWE, MKBJN-MI-PWE and MKBJN-MI-PWSD) with uncompensated counterparts (SNR-PWE, MI-PWE and MI-PWSD) and the wideband impulse waveform (WI) in the presence of MKB-NBJ.

At $P_{cd} = 0.80$, the MKBJN-SINR-PWE achieves a performance gain of 4 dB over its jammer uncompensated counterpart with single and multiple transmissions.

H. JAMMER NULLING AND JAMMER-UNCOMPENSATED ADAPTIVE WAVEFORM PERFORMANCE COMPARISON SUMMARY

1) CLASSIFICATION PERFORMANCE IN THE PRESENCE OF TIME AND FREQUENCY STATIC JAMMER DISTRIBUTIONS

The noise jammers that remain fixed in time and frequency space includes the narrowband jammers NBJ-1, NBJ-2 and NBJ-3 as well as the comb jammer CMJ. The classification performance gain of jammer nulling adaptive waveforms over jammer-uncompensated waveforms in the presence of this

jammer noise depends heavily on the jammer PSD relative to the target's frequency response. Significant classification performance improvements of jammer nulling waveforms are observed when the jammer noise is placed in the portions where the target's frequency response is large. This is evident in the P_{cd} results for the CRr platform in the presence of NBJ-2 and NBJ-3 as seen in Figure 17 and Figure 18 respectively. In contrast, marginal to moderate performance gain is achieved in the presence of noise jammers (e.g. NBJ-1) that jam target frequency response components with lower energy (see Figure 16). The smaller performance gain in this case is largely due to the fact that the target is not jammed at frequencies that contain high energy frequency response components (by NBJ-1). In other words, the impact of narrowband jammers on the classification performance of jammer-uncompensated waveforms is greater for noise jammers that jam high energy components of the target's frequency response.

The classification performance results for all waveforms in the presence of a narrowband or comb jammer (see Figure 16-19) show that the JN-SINR-PWE produces the best P_{cd} in many cases.

2) CLASSIFICATION PERFORMANCE IN THE PRESENCE OF TIME OR FREQUENCY VARYING JAMMER DISTRIBUTIONS

The noise jammers with time or frequency varying distribution include the frequency sweep SWJ, frequency agile FQJ and pulse jammers PJ. The jammer nulling adaptive waveforms outperform their jammer-uncompensated counterparts in the presence of the abovementioned noise jammers as seen in Figure 20-22. However, all jammer nulling waveforms produce comparable P_{cd} in the case with the JN-MI-PWSD achieving a slightly higher classification performance over the other jammer nulling waveforms. Likewise, the P_{cd} of jammer-uncompensated waveforms is similar in the presence of frequency sweep or frequency agile jammer noise (see Figure 20 and Figure 21). The classification performance of SNR-PWE achieves a higher P_{cd} over the other jammer-uncompensated waveforms in the presence of pulse jammer noise (see Figure 22).

3) CLASSIFICATION PERFORMANCE OF PLATFORM SPECIFIC JAMMER

The base jammer is a platform specific noise jammer considered in this paper. Here, we assume that at every simulation, the base jammer mounted on the true target hypothesis is transmitting barrage jammer noise directed at the CRr platform. The classification performance of the jammer nulling and jammer-uncompensated waveforms for a base jammer on each of the target hypothesis in Figure 23 suggests that jammer nulling waveforms perform significantly better than their jammer-uncompensated counterparts when jammer noise is transmitted by targets with smaller RCS responses; and likewise there is little to no performance gain when jammer noise is transmitted by targets with higher RCS returns. Indeed this is because target's with large RCS require larger interference

power to be jammed effectively. For the case where the target hypothesis and hence the base jammer platform is chosen randomly, the jammer nulling waveforms are observed to outperform the jammer-uncompensated waveforms (see Figure 24).

4) CLASSIFICATION PERFORMANCE IN THE PRESENCE OF KNOWLEDGE-BASED JAMMER

As seen in Figure 25 and Figure 26, the classification performance gain of jammer nulling adaptive waveforms over jammer-uncompensated waveforms is greater in the presence of KB-NBJ interference compared to the case where MKB-NBJ interference is present. There is a smaller performance gain for jammer nulling waveforms over jammer-uncompensated waveforms in MKB-NBJ noise as the MKB-NBJ not only obscure the targets' frequency response band with the greatest response energy, its jammer PSD shape matches that of each target's frequency response in their dominant frequency response band.

The classification performance results for all waveforms in the presence of KB-NBJ and MKB-NBJ (see Figure 25 and Figure 26) show that SINR-based waveforms, KBJN-SINR-PWE and MKBJN-SINR-PWE, produce the best P_{cd} in most cases.

X. SUMMARY AND CONCLUSION

In this paper, we consider the application of CRr in the EW domain. The CRr provides ES and EP support and is pitted against a comprehensive list of noise jammers and a newly introduced but highly effective target response-based knowledge-based jammer. The CRr provides ES and EP support by the use of new jammer nulling transmit-adaptive waveforms that utilize SINR and MI metrics for aircraft RCS response recognition. The noise jammers are described by various time and/or frequency distributions. High-fidelity aircraft target responses generated from CST using CAD models were utilized.

Two forms of knowledge based jammers designs were introduced, a traditionally shaped KB-NBJ with a Hamming function PSD in each narrowband lobe, and the MKB-NBJ where the narrowband jammer PSD shape is ''matched'' to the respectively target's frequency response. Apart from the two knowledge-based jammers, several other noise jammers are considered to simulate the effectiveness of adaptive waveforms. This includes the narrowband and comb jammers with a jammer frequency distribution that remains fixed in the time and frequency domain; the frequency sweep and frequency agile jammer where the jammer PSD hops its position in the frequency domain; the pulse jammer with a jammer frequency spectrum that only affects certain transmissions; and the base jammer which is platform specific.

We examine the classification performance of jammer nulling transmit-adaptive waveforms designed to mitigate the effects of noise jammers and compared their performance to jammer-uncompensated transmit-adaptive waveforms and the receive-adaptive WI pulse waveform. The results from

simulations showed that there is modest to significant improvement for jammer nulling waveform over the uncompensated waveforms and the receive-adaptive WI waveform. The extent of performance gain depends on the jammer noise frequency distribution relative to the target's energy distribution in the frequency domain and the overall target RCS response magnitude.

REFERENCES

[1] D. Adamy, *EW 101: A First Course in Electronic Warfare*. Boston, MA, USA: Artech House, 2001.

[2] S. A. Vakin, *Fundamentals of Electronic Warfare*. Boston, MA, USA: Artech House, 2001.

[3] R. A. Poisel, *Electronic Warfare Receivers and Receiving Systems*. Norwood, MA, USA: Artech House, 2014.

[4] A. E. Spezio, "Electronic warfare systems," *IEEE Trans. Microw. Theory Techn.*, vol. 39, no. 5, pp. 1578–1597, Sep. 1993.

[5] S. Haykin, "Cognitive radar: A way of the future," *IEEE Signal Process. Mag.*, vol. 23, no. 1, pp. 30–40, Jan. 2006.

[6] M. L. Manna, P. Stinco, M. Greco, and F. Gini, "Design of a cognitive radar for operation in spectrally dense environments," in *Proc. IEEE Radar Conf.*, Apr./May 2013, pp. 1–6.

[7] P. Stinco, M. S. Greco, and F. Gini, "Spectrum sensing and sharing for cognitive radars," *IET Radar, Sonar Navigat.*, vol. 10, no. 3, pp. 595–602, 2016.

[8] J. R. Guerci, *Cognitive Radar: The Knowledge-aided Fully Adaptive Approach*. Norwood, MA, USA: Artech House, 2010.

[9] N. A. Goodman, P. R. Venkata, and M. A. Neifeld, "Adaptive waveform design and sequential hypothesis testing for target recognition with active sensors," *IEEE J. Sel. Topics Signal Process.*, vol. 1, no. 1, pp. 105–113, Jun. 2007.

[10] M. R. Bell, "Information theory and radar: Mutual information and the design and analysis of radar waveforms and systems," Ph.D. dissertation, Dept. Eng. Appl. Sci., California Inst. Technol., Pasadena, CA, USA, 1988.

[11] M. R. Bell, "Information theory and radar waveform design," *IEEE Trans. Inf. Theory*, vol. 39, no. 5, pp. 1578–1597, Sep. 1993.

[12] D. DeLong and E. Hofstetter, "On the design of optimum radar waveforms for clutter rejection," *IEEE Trans. Inf. Theory*, vol. IT-13, no. 3, pp. 454–463, Jul. 1967.

[13] S. U. Pillai, H. S. Oh, D. C. Youla, and J. R. Guerci, "Optimum transmit-receiver design in the presence of signal-dependent interference and channel noise," *IEEE Trans. Inf. Theory*, vol. 46, no. 2, pp. 577–584, Mar. 2002.

[14] S. Kay, "Optimal signal design for detection of Gaussian point targets in stationary Gaussian clutter/reverberation," *IEEE J. Sel. Topics Signal Process.*, vol. 1, no. 1, pp. 31–41, Jun. 2007.

[15] J. R. Guerci and S. U. Pillai, "Theory and application of optimum transmit-receive radar," in *Proc. IEEE Int. Radar Conf.*, May 2000, pp. 705–710.

[16] D. A. Garren, M. K. Osborn, A. C. Odom, J. S. Goldstein, S. U. Pillai, and J. R. Guerci, "Enhanced target detection and identification via optimised radar transmission pulse shape," *IEE Proc.-Radar, Sonar Navigat.*, vol. 148, no. 3, pp. 130–138, Jun. 2001.

[17] R. A. Romero, J. Bae, and N. A. Goodman, "Theory and application of SNR and mutual information matched illumination waveforms," *IEEE Trans. Aerosp. Electron. Syst.*, vol. 47, no. 2, pp. 912–927, Apr. 2011.

[18] R. A. Romero and N. A. Goodman, "Information-theoretic matched waveform in signal dependent interference," in *Proc. IEEE Radar Conf.*, May 2008, pp. 1–6.

[19] A. Aubry, A. DeMaio, A. Farina, and M. Wicks, "Knowledge-aided (potentially cognitive) transmit signal and receive filter design in signal-dependent clutter," *IEEE Trans. Aerosp. Electron. Syst.*, vol. 49, no. 1, pp. 93–117, Jan. 2013.

[20] J. Bae and N. A. Goodman, "Automatic target recognition with unknown orientation and adaptive waveforms," in *Proc. IEEE Radar Conf.*, May 2011, pp. 1000–1005.

[21] Q. J. O. Tan, R. A. Romero, and D. C. Jenn, "Target recognition with adaptive waveforms in cognitive radar using practical target RCS responses," in *Proc. IEEE Radar Conf.*, Apr. 2018, pp. 606–611.

[22] K. L. Bell, C. J. Baker, G. E. Smith, J. T. Johnson, and M. Rangaswamy, "Fully adaptive radar for target tracking Part I: Single target tracking," in *Proc. IEEE Radar Conf.*, May 2014, pp. 303–308.

[23] K. L. Bell, C. J. Baker, G. E. Smith, J. T. Johnson, and M. Rangaswamy, "Fully adaptive radar for target tracking Part II: Target detection and track initiation," in *Proc. IEEE Radar Conf.*, May 2014, pp. 309–314.

[24] P. Nielsen and N. A. Goodman, "Integrated detection and tracking via closed-loop radar with spatial-domain matched illumination," in *Proc. Int. Conf. Radar*, Sep. 2008, pp. 546–551.

[25] T. B. Butler and N. A. Goodman, "Multistatic target classification with adaptive waveforms," in *Proc. IEEE Radar Conf.*, May 2008, pp. 1–6.

[26] R. A. Romero and N. A. Goodman, "Cognitive radar network: Cooperative adaptive beamsteering for integrated search-and-track application," *IEEE Trans. Aerosp. Electron. Syst.*, vol. 49, no. 2, pp. 915–931, Apr. 2013.

[27] Q. J. O. Tan and R. A. Romero, "Air vehicle target recognition with jammer nulling adaptive waveforms in cognitive radar using high-fidelity RCS responses," in *Proc. Int. Conf. Radar*, Aug. 2018, pp. 1–6.

[28] Q. J. O. Tan and R. A. Romero, "Jammer nulling adaptive waveforms with cognitive radar for aircraft RCS recognition in presence of frequency sweep and base jammers," in *Proc. Asilomar Conf. Signals, Syst., Comput.*, Oct. 2018, pp. 1339–1343.

[29] J. Y. Nieh and R. A. Romero, "Comparison of ambiguity function of eigen-waveform to wideband and pulsed radar waveforms: A comprehensive tutorial," *J. Eng.*, vol. 2017, no. 4, pp. 203–221, Apr. 2018.

[30] A. W. Graham, *Communications, Radar and Electronic Warfare*. Hoboken, NJ, USA: Wiley, 2008.

[31] R. A. Romero, "Detection performance of matched transmit waveform for moving extended targets," in *Proc. Asilomar Conf. Signals, Syst., Comput.*, 2013, pp. 1956–1960.

[32] J. Bae and N. A. Goodman, "Adaptive waveforms for target class discrimination," in *Proc. Int. Waveform Diversity Design Conf.*, 2007, pp. 395–399.

[33] J. Bae and N. A. Goodman, "Evaluation of modulus-constrained matched illumination waveforms for target identification," *IEE Proc. F Commun., Radar Signal Process.*, vol. 129, no. 3, pp. 93–117, Jan. 2013.

[34] P. M. Grant and J. H. Collins, "Introduction to electronic warfare," *IEE Proc. F-Commun., Radar Signal Process.*, vol. 129, no. 3, pp. 113–132, 1982.

[35] M. I. Skolnik, *Radar Handbook*, 3rd ed. New York, NY, USA: McGraw-Hill, 2008.

[36] R. N. Lothes, *Radar Vulnerability to Jamming*. Boston, MA, USA: Artech House, 1990.

Q. JEANETTE O. TAN (S'17–M'19) received the B.S.E.E. degree from the National University of Singapore, Singapore, in 2010, the M.S. degree in information warfare systems engineering from the Naval Postgraduate School, Monterey, CA, USA, in 2015, and the Ph.D. degree in electrical and computer engineering from the Naval Postgraduate School, Monterey, CA, USA, in 2019. She is currently a Senior Research Engineer with the Electronic Systems Division, DSO National Laboratories, Singapore.

RIC A. ROMERO (S'07–M'10–SM'12) received the B.S.E.E. degree from Purdue University, West Lafayette, IN, USA, in 1999, the M.S.E.E. degree from the University of Southern California, Los Angeles, CA, USA, in 2004, and the Ph.D. degree in electrical and computer engineering from The University of Arizona, Tucson, AZ, USA, in 2010.

He was a Senior Multidisciplined Engineer II with Raytheon Missile Systems, Tucson, from 1999 to 2010. He was involved in various communications, radar, and research and development programs. He was also a Graduate Research Assistant with the Laboratory for Sensor and Array Processing, The University of Arizona, from 2007 to 2010. He is currently an Associate Professor with the Department of Electrical and Computer Engineering, Naval Postgraduate School, Monterey, CA, USA. His research interests include the general areas of radar, sensor information processing, and communications.

Dr. Romero was awarded the 2004 Corporate Excellence in Technology Award, which is a company-wide technical prize at Raytheon Corporation. He was also granted the Raytheon Advanced Scholarship Program Fellowships, from 2002 to 2004 and from 2005 to 2007.

• • •